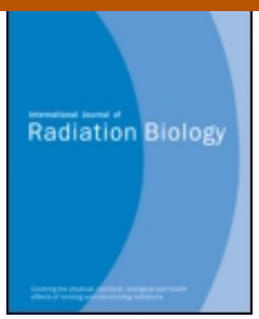

International Journal of Radiation Biology

ISSN: 0955-3002 (Print) 1362-3095 (Online) Journal homepage: http://www.tandfonline.com/loi/irab20

Development of a small-animal focal brain irradiation model to study radiation injury and radiation-injury modifiers

Katalin Hideghéty, Imola Plangár, Imola Mán, Gábor Fekete, Zoltán Nagy, Gábor Volford, Tünde Tőkés, Emilia Szabó, Zoltán Szabó, Kitti Brinyiczki, Petra Mózes & István Németh

To cite this article: Katalin Hideghéty, Imola Plangár, Imola Mán, Gábor Fekete, Zoltán Nagy, Gábor Volford, Tünde Tőkés, Emilia Szabó, Zoltán Szabó, Kitti Brinyiczki, Petra Mózes & István Németh (2013) Development of a small-animal focal brain irradiation model to study radiation injury and radiation-injury modifiers, International Journal of Radiation Biology, 89:8, 645-655, DOI: 10.3109/09553002.2013.784424

To link to this article: https://doi.org/10.3109/09553002.2013.784424

Accepted author version posted online: 13 Mar 2013.
Published online: 16 Apr 2013.

International Journal of Radiation Biology, August 2013; 89(8): 645–655

ISSN 0955-3002 print / ISSN 1362-3095 online
DOI: 10.3109/09553002.2013.784424

informa
healthcare

Development of a small-animal focal brain irradiation model to study radiation injury and radiation-injury modifiers

Katalin Hideghéty[1], Imola Plangár[2], Imola Mán[3], Gábor Fekete[1], Zoltán Nagy[1], Gábor Volford[4], Tünde Tőkés[5], Emilia Szabó[3], Zoltán Szabó[1], Kitti Brinyiczki[6], Petra Mózes[1] & István Németh[3]

Departments of [1]Oncotherapy, [2]Neurology, [3]Dermatology and Allergology and [4]Radiology, and Institutes of [5]Surgical Research and [6]Pathology, Faculty of Medicine, University of Szeged, Szeged, Hungary

Abstract

Purpose: **Our aim was to establish an effective small-animal focal brain radiation model for research on brain injuries.**

***Material and methods*: Groups of up to six rats were exposed to a range of doses from 120–40 Gy, at 10 intervals of a 6 MeV electron beam. Open-field motor functions and water maze learning-memory tests were performed after the irradiation at two-week intervals. Morphological changes were detected through repeated magnetic resonance imaging (MRI) monthly and were compared with the histopathological findings to determine if they predicted late microscopic changes.**

Results: **The development of necrosis proved to be dose-dependent. 120 Gy resulted in serious deterioration within 4 weeks in all rats. Localized necrosis in one hemisphere was detected 2 months after the irradiation with ≥70 Gy, and 3 months after 40–60 Gy consistent for all animals. The Morris water maze (MWM) tests proved to be the most sensitive tool for the early detection of a brain functional impairment. MRI screening provided useful information on the development of radiation necrosis, which defined the time point for histological examinations.**

Conclusions: **The described method permits accurate dose delivery to a definite part in one hemisphere of the brain for six rats at a time. Following complex examinations, a dose of 40 Gy and a follow-up time of 4 months are proposed for investigations on neuroradiation modifiers.**

Keywords: Focal irradiation, brain, rat

Introduction

Radiation therapy plays an indispensable role in the management of sinonasal, nasopharyngeal, and both primary and secondary brain tumors. However, its side-effects, and in particular the acute and chronic brain injuries, are major dose-limiting complications inhibiting effective treatment of such tumors. After recovery from the early-onset syndromes, the late effects (from 3 months to 10 years after irradiation, but mainly in the first 2 years) are irreversible and devastating. The late reactions occur as secondary to damage to vascular and glial tissues, which develop due to cytokine release, increases in capillary permeability and extracellular edema, and demyelination leading to small-vessel occlusive disease and bleeding (Fike et al. 1984, 2009, Tofilon and Fike 2000, Belka et al. 2001, Monje and Palmer 2003, Wong and Van der Kogel 2004, Hwang et al. 2006). Severe late central nervous system toxicity has been reported in 2–32% of the patients, with a $< 5\%$ incidence after standard 60 Gy in 1.8–2 Gy fractions (Emami et al. 1991, Ruben et al. 2006) and up to 32% following radiosurgery (Williams et al. 2009, Marks et al. 2010). Considerable effort has been devoted to reducing the risk of dose-dependent minor-to-severe neurocognitive deficits and focal radiation necrosis, with the subsequent progressive deterioration and death. The currently emerging external beam techniques, such as stereotactic radiosurgery, conformal and intensity-modulated teletherapy, helical tomotherapy, volumetric arc therapy and proton therapy, increase the physical selectivity or complexity (simultaneous integrated boost) of the dose delivery. At the same time, the higher fraction doses or higher relative biological effectivity are associated with a higher probability of radiation necrosis (Chua et al. 2009, Blonigen et al. 2010, Mizumoto et al. 2010, Kase et al. 2011, Minniti et al. 2011). Moreover, in a majority of the cases the inclusion of surrounding normal brain tissue into the clinical target volume cannot be avoided, because of the potential tumor cell content. A different approach, involving increase of the radiation tolerance of the healthy brain cells, therefore appears to be of great importance (Jenrow et al. 2010, Robbins et al. 2010, Xin et al. 2012).

Investigations of the potential protective effect of different drugs demand the availability of a reproducible and reliable small-animal experimental model of partial brain irradiation with the comparative detection of functional and morphological changes in a reasonable time frame.

Correspondence: Katalin Hideghéty, MD, PhD, Department of Oncotherapy, Albert Szent-Györgyi Clinical Center, University of Szeged, Korányi fasor 12, H-6720 Szeged, Hungary. Tel: + 36 62 545404. Fax: + 36 62 545922. E-mail: katalin.hideghety@gmail.com

(Received 6 November 2012; revised 8 February 2013; accepted 5 March 2013)

In the small-animal radiobiological studies on brain injury to date, either the whole brain was irradiated, with or without shielding of the susceptible neighboring organs (ocular, oral and pharyngeal structures), or very special, time-consuming techniques were applied to achieve focal energy deposition in the rat brain (stereotaxic radiotherapy, proton stereotaxy or synchrotron-based microbeam irradiation). The aim of the present study was the development of a relatively simple, but reproducible and effective experimental system that could become widely available for research on focal brain injury due to radiotherapy or concomitant radio-chemotherapy, and for preclinical studies on potential radio-neuroprotective agents.

Materials and methods

Animals

Experiments were performed on 57 adult Sprague-Dawley male rats, weighing on average 210 g (range 176–280 g). The animals were housed in a climate-controlled environment (25°C) maintained on a 12 h light/12 h dark cycle and were allowed free access to food and water. All experiments were conducted in full accordance with the European Communities Council Directive of 24 November 1986 (86/609/EEC) for the Care and Use of Laboratory Animals and were approved by the University Animal Research Committee.

Dosimetry of small electron field

In order to verify the dose depth curve, the field profile and the lateral dose fall-off of the 2, 4, 6, 8, 10 and 12 mm electron collimators, we measured the absorbed dose of a 6 MeV electron beam irradiating at a dose rate of 300 monitor units (MU)/min in a water phantom, using a pin-point ionization chamber (Canberra packard Central Europe GmBH, Schwadorf Austria), and in a solid water phantom with a 1 cm build-up layer for film dosimetry (Canberra packard Central Europe GmBH). The graphical representation of the entrance of the treatment beam was aligned with the approximate location of the corpus callosum-hippocampus as determined from pre-existing magnetic resonance imaging (MRI) and computed tomography (CT) scan of a rat. Thus, for evaluation of the dose distribution, the 90% and 70% isodose levels were superimposed on the image of the skull, aligned with the approximate location of the general rat brain structures (Figure 1A).

Irradiation

Two prone adult male Sprague-Dawley rats placed nose-to-nose in the irradiation position, with earpin fixation, were imaged in the Emotion 6 CT scanner (Siemens AG, Erlangen Germany) in order to obtain three-dimensional anatomical information for planning of the radiation geometry. Slices (1.25 mm) were obtained by using the maximum resolution afforded by the scanner. The whole brain, eyes, internal ears, corpus callosum and hippocampus on both sides, together with the target volume, were delineated in the XIO CMS™ treatment planning system (ELEKTA, Stockholm, Sweden), using MRI and the anatomy atlas of the rat brain. A 6 MeV lateral electron beam at a 100 cm source-to-skin distance (SSD) was chosen because it has a sharp dose fall-off with depth, confining the radiation dose delivery to the defined volume of the hippocampus, including the corpus callosum of the ipsilateral hemisphere, while sparing the skin, the eyes, the ears, the cerebellum, the frontal lobe and the contralateral half of the brain (Figure 1A, 1B). No build-up bolus was used.

The planned doses were delivered in a single fraction by means of a linear accelerator (Primus IMRT, Siemens, Erlangen, Germany) at a dose rate of 300–900 MU/min, with six circular apertures, 10 mm in diameter each in a 20 mm thick Newton metal insert placed into the 15×15 cm electron applicator, to the following groups of animals: 120 Gy ($n = 3$), 110 Gy ($n = 3$), 100 Gy ($n = 3$), 90 Gy ($n = 6$), 80 Gy ($n = 3$), 70 Gy ($n = 6$), 60 Gy ($n = 3$), 50 Gy ($n = 6$), 40 Gy ($n = 12$), sham irradiated ($n = 12$), respectively.

Immediately prior to irradiation, the animals were anesthetized with an intraperitoneal (i.p.) injection of 4% chloral hydrate (1 ml/100 g Fluka Analytical, Buchs, Switzerland, 23100). They were placed two-by-two, nose-to-nose, on the three-storeyed positioning device on the couch of the irradiation unit and their heads were aligned individually at the intersection of the beam axis-marking lasers. The light field was directed at exactly the middle of the distance between the eye and ear, with the upper edge at the top of the skull. An ear plug was inserted into the ipsilateral ear. Pairs of animals were situated on all three storeys. The irradiation dose rate

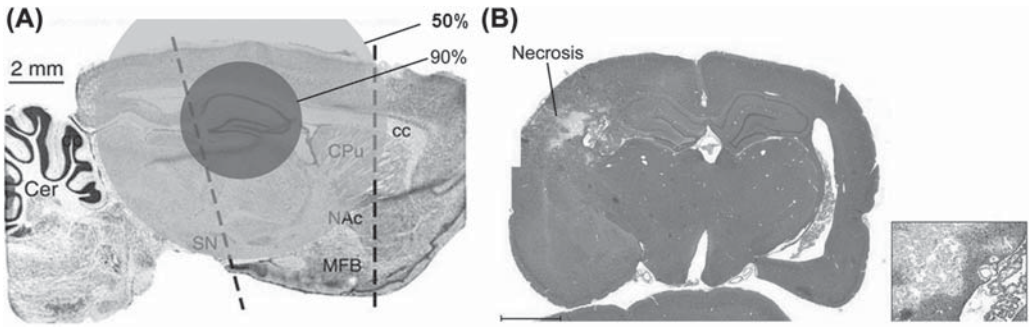

Figure 1. Dose distribution using a 10 mm diameter beam. The 90% and 70% isodose levels are superimposed on the sagittal image of the rat brain (A). The H&E slide of the brain at the 70 Gy dose level. Damage caused by the irradiation at the left side localized to a defined small brain volume in the high dose region without any histopathological aberrations in the contralateral hemisphere (B). The sub-panel image right to the image B shows the post irradiation brain injury with higher magnification. Cer, cerebellum; SN, substantia nigra; CPu, caudate putamen; NAc, nucleus accumbens; MFB, medial forebrain bundle; cc, corpus callosum.

was 300/900 MU/min and de-escalated doses ranging from 120–40 Gy were applied, with 3–12 animals per dose level. The monitor units (3000 MU/10 Gy) used for the irradiation were derived from the previous small-field dosimetry. The radiation geometry was verified prior to the irradiation, and documented by control imaging on film after the irradiation. The animals were first imaged with the 6-hole insert exposed to 6 MeV electrons (50 MU), after which the insert was removed and a large field (20×20 cm) of 6 MeV photons was imaged (1.6 MU) to obtain an outline of the skull together with the body landmarks such as oral cavity, ear canals, etc. Sham controls were anesthetized, but not imaged or irradiated. Following treatment, the animals were transferred to their home cages and kept under standard conditions, with weekly weight measurements, descriptive behaviour observations and skin detection.

Neurofunctional tests

Rats were placed individually in cages, taken to the behavioural room (ventilated and maintained at 21–23°C) and allowed to habituate for 1 h prior to behavioural testing, which was performed during the light phase of the light/dark cycle. The neurofunctional examinations were performed prior to (baseline), and every two weeks (open field) or monthly (Morris water maze (MWM)) after the radiation (Additionally MWM test was repeated more frequently during the first month post-irradiation). All arenas and objects used in the neurofunctional experiments were cleaned with 70% alcohol after each trial. The test devices were dried before the next task started. Feces were removed from the MWM between trials. All tests were recorded with a video camera.

Open field

Locomotor activity was measured every 2 weeks by an automated tracking system with an activity chamber. A monochrome video camera was mounted at the top of the chamber. The open black box with a dark floor was made of wood ($48 \times 48 \times 40$ cm, length $\times$ width $\times$ height). The box was connected to a computer which recorded the inquisitive behaviour and locomotor activity of the animal. The rats were placed individually into the arena, which was equipped with automated infrared photocells for measurements, and allowed to move spontaneously for 15 min. Tests were performed at the same time of the day so as to minimize changes in locomotor activity due to the diurnal rhythm. Between sessions, the open-field was cleaned with alcohol and dried. The movement signals (stored in the computer) were analyzed by Conducta 1.0 (Experimetria Ltd, Budapest, Hungary) analysis software. The analysis resulted in a track record; the locomotor activity was expressed as the total distance moved (cm) in a predetermined period of time, the times spent in movement and at rest (s), the average speed of the rat (cm/s), and the frequency and duration of prancing.

Morris water maze

The MWM protocol of Vorhees and Willams (Vorhees and Williams 2006) was used, visuospatial cues being provided to guide the animals in tests of hippocampal memory. The MWM consisted of a cylindrical white tank with a diameter of 175 cm and height of 50 cm, made opaque with non-toxic tempera paint. The tank was filled with water up to 32.5 cm and maintained at 21–24°C. The pool was divided into four quadrants, arbitrarily referred to as south-east, north-east, north-west and south-west quadrants. A transparent square Perspex escape platform measuring 10×10 cm was submerged 1 cm below the surface of the water (where it was not visible to the animals), 30 cm from the wall in the south-east quadrant of the pool. The position of the platform was constant throughout the 3-day acquisition period. Four A3-sized pictures (black, white and blue circles, triangles, stripes and squares) were fixed permanently on the surrounding walls and served as distal navigation cues to enable the rats to locate the platform. The distinctive visual cues remained constant throughout the entire course of testing. The first two days were acquisition or training days, and the task was performed on the third day. The training period consisted of five trials per day with a 5-min inter-trial interval. Each trial began with the rat in the pool and ended when the rat found the platform or after 120 s. If the animal failed to locate the platform within 120 s, it was guided to the platform manually. Once on the platform, the rat was allowed to rest for 10 s. It was then towel-dried and placed in an inter-trial holding cage where a heating source was provided to maintain the animal's body temperature during the inter-trial interval. During the acquisition phase, measurements were made of the time (s) and the path length (cm) taken to locate the platform.

MRI

Sixty rats underwent 72 MRI procedures prior to or 4–19 weeks after irradiation. Randomly selected animals from each irradiation dose level were examined by means of 1.5 T MRI (Signa Excide HDxT, GE Healthcare, Little Chalfont, Buckinghamshire, UK), using a human head coil with a home-made styrofoam holder containing six animals under i.p. chloral hydrate (Sigma Aldrich, St Louis, MO, USA) anesthesia. No contrast agent was used for MRI images. Twelve animals underwent three MRI examinations, at baseline, mid-term and prior to histology: coronal-T1 (T1: longitudinal relaxation time) (3 dimension [3D] ultrafast gradient echo with magnetization preparation [IR-FSPGR], field of view [FOV] 17.0 mm^2, inversion time [TI] 450 slice thickness [ST]: 1.2 mm), sagittal (3D Cube T2, repetition time [Tr] 3000, echo time [TE] 60, FOV: 13 mm^2, TI 450, ST: 1.2 mm, Space [Sp]: 0) and coronal T2 (T2: transverse relaxation time) weighted (3D IR-FSPGR; FOV: 13 mm^2, ST: 1.2 mm, Sp: 0) images were acquired. The MRI procedure required about 10 min per sequence.

Histopathology

Rats were anesthetized with 4% chloral hydrate and perfused transcardially with 0.1 M phosphate buffer solution (pH 7.0–7.4) to flush out the blood before they were fixed with 4% paraformaldehyde buffer solution (pH 7.0–7.4) at 4°C. The brains were dissected out and fixed in paraformaldehyde for 1 day before being embedded in paraffin. Serial 3 μm thick sections were cut with a vibratome. Multiple sections were stained with hematoxylin and eosin (H&E) for histologic evaluation; for the demonstration of demyelination,

Luxol fast blue (LFB) staining was used. All analyses were performed blindly, using coded sections. Evaluations were carried out independently by two experienced histopathologists with a semiquantitative method, a score being awarded for each examined parameter (necrosis, macrophage density, vascularization, hemorrhage, reactive gliosis, calcification and demyelination), on a semiquantitative scale from 1–4 (whereas '1' represented the normal brain structure).

In the case of necrosis, at low magnification (optical magnification [OM] 50×): 0: not detected; 1: necrosis detected in $<50\%$ of the examined field; 2: necrosis detected in 50–100% of the examined field; 3: the necrosis detected was larger than the field of vision, or affected both hemispheres of the brain. The macrophage density was examined at high magnification (OM 400×): 0: no foamy macrophages detected; 1: <5 foamy macrophages/high-power field (HPF); 2: 5–10 macrophages/HPF; 3: >10 macrophages/HPF. Vascularization was scored (OM 50×) as 0: no neovascularization detected; 1: newly-formed small, simple capillaries detected around the necrosis; 2: newly-formed capillaries detected around the necrosis, which contained variously-sized, but simple capillaries; 3: large, complex capillaries or small capillaries seen with endothelial proliferation. Hemorrhage (OM 50×): 0: no hemorrhage detected; 1: hemorrhage detected in a single, small focus; 2: hemorrhage seen in multiple small foci, or a single, larger focus; 3: extensive multiple hemorrhage detected. Reactive gliosis (OM 200×): 0: no; 1: mild; 2: moderate; 3: severe reactive gliosis detected in the brain. Calcification (OM 50×): 0: no calcification; 1: a single small calcified focus detected; 2: multiple small or a single, larger focus detected; 3: extensive, multiple calcifications detected. Demyelination (OM 400×): 0: none; 1: mild; 2: moderate demyelination, but fibers detected; 3: severe demyelination, with destruction of the fibers.

Statistical analysis

Statistically significant differences relative to the control are reported as $^{*}p<0.05$, $^{**}p<0.01$, $^{***}p<0.001$, while those relative to each other at different dose levels are denoted by the symbol #. Data were analyzed by using analysis of variance (ANOVA) and the Fisher PLSD *post hoc* test. Significant interactions were explored with the *t*-test (unpaired) and the Mann-Whitney rank sum test when appropriate.

Results

At the dose levels ranging from 90–40 Gy, the morphological and functional changes could be evaluated, but outside this dose range we observed either lethal or serious events (from 120–100 Gy) or no changes (doses <30 Gy; data not reported here) during the at most 4-month post-irradiation follow-up period.

Subject outcome

At the highest dose (120 Gy), all of the animals underwent a rapid serious general and neurofunctional decline (Figure 2) and died or had to be euthanized between 25 and 40 days after the irradiation. The rats irradiated at the 110 Gy dose level survived longer, but also deteriorated between 30 and 50 days post-irradiation. At the lower dose levels, there were no signs of a general impairment; the weight gain, eating habits and daily activity did not differ from those of the control rats. All the irradiated animals suffered hair loss from the site corresponding to the beam entrance within 30 days following the irradiation.

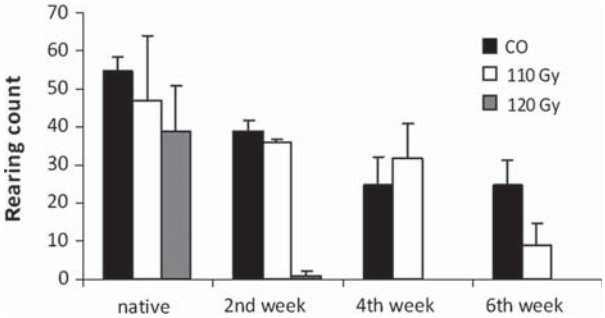

Figure 2. The explorative behavior of the animals started to decrease 2 weeks after irradiation at the 120–110 Gy dose levels, but the rats died before marked changes in this parameter occurred (mean ± SEM).

Neurofunctional tasks

In the early observations, significant differences in the locomotor function of the rats irradiated at 90–40 Gy were not detected with the open-field test (either in the ambulation time or in the mean velocity), but the motor activity started to decrease slightly 8 weeks after irradiation with the 90 Gy dose. The prancing activity was significantly reduced in the groups that received 90–60 Gy. The time at which the rearing activity started to decline was dose-dependent: It was 40–55 days post-irradiation after the 90 Gy dose (mean ± standard error of the mean [SEM], $^{*}p<0.05$) (Figure 3). The animals that received 120 Gy died before marked changes could be seen in this parameter.

The MWM test was found to be a highly sensitive tool for the detection of a neurofunctional impairment. A relevant memory deterioration was detected soon after the dose delivery at the 70 Gy dose level and the difference increased with time ($^{***}p<0.001$). A significant cognitive deficit was also observed 8 weeks after the irradiation in the group treated with 60 Gy (mean ± SEM, $^{*}p<0.05$) (Figure 4). The starting of the impairment of the learning-memory function proved to be dose-dependent; in the groups irradiated at 50–40 Gy, the first sign of deterioration was detected 30 days post-irradiation and the difference relative to the control animals was more pronounced after 90 days (Figure 5).

MRI

Serial MRI revealed structural damage in the form of cavity formation in the cortical region, with extensive perifocal edema, which appeared in general from 2–4 months following irradiation (Figure 6). Changes may have occurred earlier but we performed the first post-irradiation MRI after 4 weeks in the majority of the cases, since our aim was to investigate late effects. Radiation-induced cystic necrosis began to appear at approximately 4–8 weeks post-irradiation in the rats irradiated with 120–60 Gy; after a lower dose, the structural changes emerged later, 19–24 weeks after irradiation: in

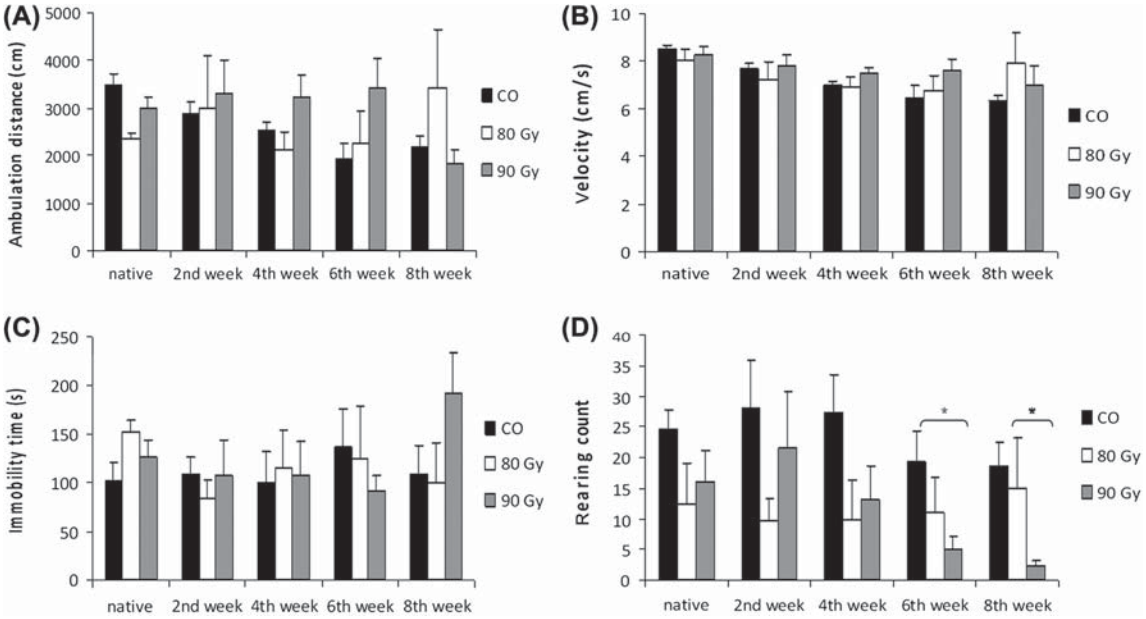

Figure 3. At the 90 Gy dose level, significant changes in ambulation ability were detected after 6 and 8 weeks. The number of rearings also decreased in the 90 Gy group relative to the control. The mean velocity and the immobility time of the rats did not change markedly (mean ± SEM; $^{*}p < 0.05$).

the T2 weighted images of the ipsilateral hemisphere, in both the coronal and the sagittal plane (Figure 7).

Histopathological findings

The H&E-stained slides of the control animals and the non-irradiated regions of the brain of the treated animals exhibited no signs of necrosis, i.e., neither reactive astrogliosis, nor any of the other examined histopathological categories (Figure 1B). In the irradiated region of the brain, the following parameters correlated closely with the high (90–120 Gy), medium (60–80 Gy) or low dose (40–50 Gy) level: reactive gliosis, vascularization, macrophage density, necrosis and calcification. No marked dose dependence was detected as concerns the extent of hemorrhage (Figure 8D). The dose $>$ 90 Gy groups displayed severe necrosis that reached the gray and white matter, causing severe demyelination, with destruction of the fibers. The levels of necrosis, reactive astrogliosis, calcification and the density of the foamy macrophages were significantly elevated in these groups as compared with the control animals (Figure 8).

The extent of the hemorrhage was significantly higher than for the other irradiated animal groups. The scores in the 90 Gy group were as follows: Necrosis (2.83), macrophage density (2.33), neovascularization (2.50), hemorrhage (1.0), reactive astrogliosis (2.0), calcification (2.17) and demyelination (3.0). In the 60–80 Gy groups, severe-to-moderate necrosis was seen, with severe-to-moderate demyelination, but the fibers could mostly be detected. In one irradiated animal, fibrin coagulum was seen in a newly-formed capillary near the necrosis. In comparison with the control group, significant correlations were detected in the following categories: necrosis, macrophage density, vascularization, calcification and reactive gliosis. Moderate hemorrhage was observed in the animals irradiated with the 80 Gy dose. The scores were as follows: necrosis (1.89), macrophage density (2.00), neovascularization (1.89), hemorrhage (1.1), reactive astrogliosis (1.3), calcification (1.3) and demyelination

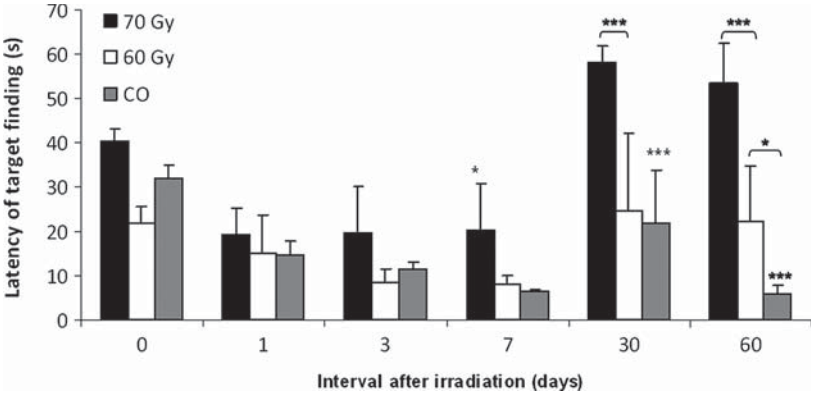

Figure 4. Memory deterioration was detected 7 days after the dose delivery at the 70 Gy dose level and the difference increased with time (mean ± SEM; $^{*}p < 0.05$, $^{***}p < 0.001$). At the 60 Gy dose level significant cognitive deficit was observed 8 weeks after the irradiation (mean ± SEM; $^{*}p < 0.05$).

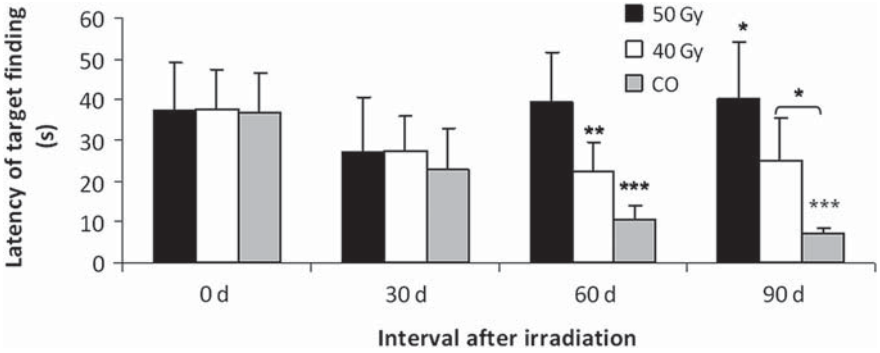

Figure 5. In the groups irradiated at 50–40 Gy, the first sign of deterioration was detected 30 days post-irradiation and the difference relative to the control animals was more pronounced after 90 days (mean ± SEM; $***p < 0.001$).

(2.2). In the 40–50 Gy groups, mild-to-moderate necrosis was detected, with mild-to-moderate demyelination. Significantly increased levels of necrosis, vascularization and reactive astrogliosis were seen. Mild calcification was revealed. Interestingly, in one animal, irradiated with the 50 Gy dose, meningoencephalitis was observed, but the presence of bacteria was not seen. The scores were as follows: Necrosis (1.45), macrophage density (1.00), neovascularization (1.00), hemorrhage (0.73), reactive astrogliosis (0.73), calcification (0.91) and demyelination (1.27).

Discussion

We have developed a simple and effective method for the delivery of a radiation dose to a well-circumscribed region of the brain of a maximum of six small animals simultaneously, and a reproducible experimental model for quantification of the functional and morphological changes occurring due to the radiation-induced focal brain damage within a reasonable time frame.

Preclinical studies on central nervous system (CNS) injuries have mainly made use of non-targeted dose delivery resulting from full-body radiation fields with the selective shielding of extracranial parts (Akiyama et al. 2001, Vinchon-Petit et al. 2010), or whole-brain irradiation using a standard field with a bolus above the skull (Ernst-Stecken et al. 2007). However, highly selective dose delivery techniques were recently introduced for humans in the cases of head and neck and primary brain tumors, and radiosurgery for benign and malignant brain lesions. For radiobiological investigations in an experimental setting corresponding to clinical radiotherapy, conformal partial brain irradiation was performed on large animals (Tiller-Borcich et al. 1987, Lunsford et al. 1990, Yamaguchi et al. 1991, Spiegelmann et al. 1993), or a sophisticated technique was applied, such as small-animal stereotactic irradiation either with a gamma knife (Yang et al. 2000, Kamiryo et al. 2001, Liscák et al. 2002, Jirák et al. 2007, Liang et al. 2008, Charest et al. 2009, Hirano et al. 2009, Massager et al. 2009a, 2009b, Marcelin et al. 2010) or with a linear accelerator (LINAC)-based approach (Ernst-Stecken et al. 2007, Lin et al. 2012). Arc therapy with the application of cylindrical collimators allows the irradiation of subregions of the skull of one subject animal (Reinacher et al. 1999, Münter et al. 2001) and the addition of image guidance of cone beam CT results in increased accuracy (Tan et al. 2011). For even more precise and highly conformal dose delivery in small animals, special devices have been developed.

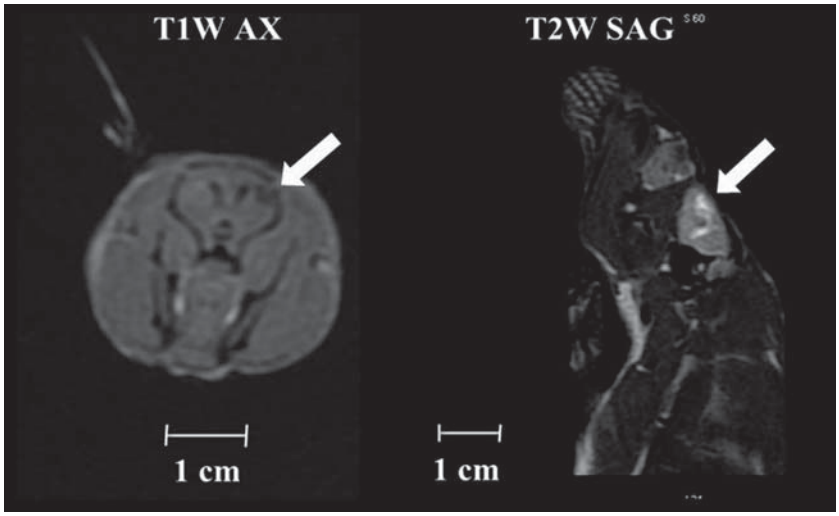

Figure 6. Serial MRI revealed visible structural damage in the form of cavity formation in the cortical region, with extensive perifocal edema, which appeared from 2–4 months following irradiation. Arrows show the place of the radiation injury. The meaning of T1W AX is T1 weighted image of the brain in axial plane and T2W SAG is T2 weighted image of the brain in sagittal plane.

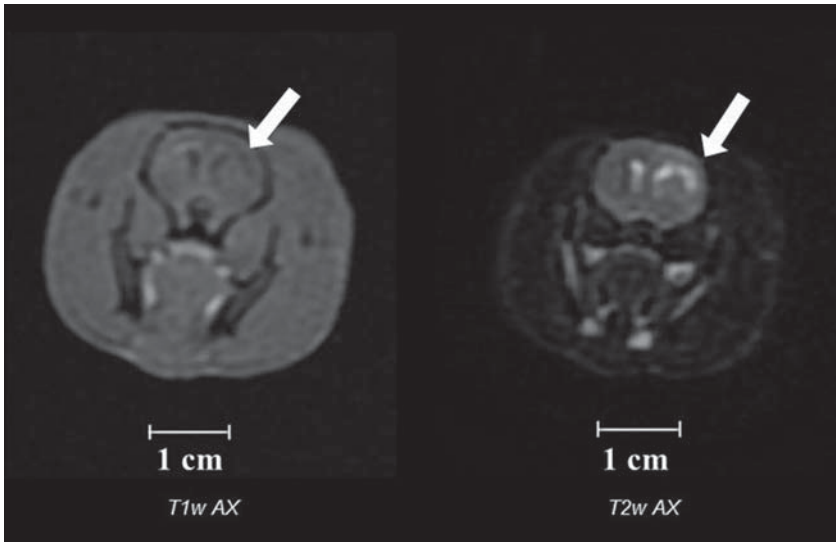

Figure 7. Radiation-induced cystic necrosis began to appear at approximately 4–8 weeks post-irradiation in rats irradiated with 120–60 Gy; at lower doses, the structural changes were observed later, 19–24 weeks after irradiation, in the T_2 weight images (T2W), in the ipsilateral hemisphere in both the coronal and sagittal planes. Arrows show the place of the radiation injury. T1W AX, T1 weighted image of the brain in axial plane; T2W SAG, T2 weighted image of the brain in sagittal plane.

The advent of improved focusing of an X-ray scalpel can be applied to brain targets as small as a few millimeters in diameter (Gutman et al. 2007). Microbeam radiation therapy involves the use of micrometer-wide synchrotron-generated X-ray beams which can provide a homogenous dose delivery to a target volume of 7 mm^3 in the rat caudate nucleus (Anschel et al. 2007). Proton beams are likewise excellent tools for the precise energy deposition of ionizing radiation to a small focus in the small-animal brain (Namba et al. 1996, Rabinov et al. 2006). The latter radiation techniques provide increased precision as concerns dose delivery to a small volume of the rat brain, though all of them are rather time-consuming and highly labour-intensive. Our method is quite a simple approach that results in the well-circumscribed irradiation of one dedicated region of the rat brain, limited to one side. We have developed a special small-animal holder where three pairs of animals can be positioned nose-to-nose on three storeys, each of which can be adjusted with submillimeter elevation precision. The equal dose delivery to the six rats is based on a custom-made insert containing six holes and six earpins with defined geometry. The film verification prior to and after the radiation provides high accuracy and quality control of the radiation.

As far as we are aware, this method involving six customized apertures 8–10 mm in diameter for 6 MeV electron beams with an SSD of 100 cm is the first approach that enables the selective irradiation of a predefined brain region, with the non-irradiated hemisphere serving as control, in multiple animal targets simultaneously. The simultaneous irradiation of more than one rat was earlier reported by Vinchon-Petit et al. (2010), but that was not a conformal method: the whole brains of four animals were treated with uniform 15×15 cm radiation fields at a source-axis distance of 100 cm. In our own previous work, we achieved conformal, simultaneous irradiation limited to one region with the use of a special immobilization device and a BrainLab stereotactic system including a micro-multileaf collimator, but the frontal lobe was irradiated equally on both sides and only two animals could be treated simultaneously (unpublished data of Farkas et al.). The group at the Sloan-Kettering Institute for Cancer Research, New York, USA, centered the full dose in the $5 \times 5 \times 5$ mm voxel of the brain tissue that comprised both hippocampi, using a 250 kV orthovoltage system equipped with a 0.25 mm copper filter and a custom-designed positioning device platform based on the standard stereotactic frame so that six animals could be irradiated simultaneously. The heads were centered in a 20×20 cm treatment field and X-irradiation was limited to an adjustable 2 cm diameter circular aperture centered over the cranium.

There was an inevitable 'spill-over' effect that included the surrounding brain tissue, but the 80–60% isodose levels declined sharply within the approximate volume of $10 \times 10 \times 10$ mm (Panagiotakos et al. 2007). Our method is comparable as regards the number of animals that can be treated at the same time, but our target volume can be limited to one hemisphere in consequence of the characteristics of the electron dose-depth curve. Because of the relatively circumscribed, reproducible energy deposition, the radiation was well tolerated in the acute phase, with minimal side-effects, including hair loss at the irradiated site. A threshold could be observed at 100 Gy in the delayed reaction because the rats irradiated with a dose > 100 Gy experienced a severe general and neurological decline within 2 months post-irradiation. At focal brain irradiation doses ≤ 100 Gy, the animals did not show any sign of a general deterioration. A similar result was published by Liscák et al. (2002), who found that, when both hippocampi were irradiated with 25, 50, 75, 100 or 150 Gy, the dose higher than 100 Gy led to serious sequalae and even death of the subject animals within 4–5 months. In the case of a 100 Gy dose delivered to a smaller volume (a spherical target volume of 3.7 mm or 4.7 mm in the right frontal lobe), the rats could be followed for up to 7 months, but then had to be sacrificed due to their general and neurological deterioration (Jirák et al. 2007).

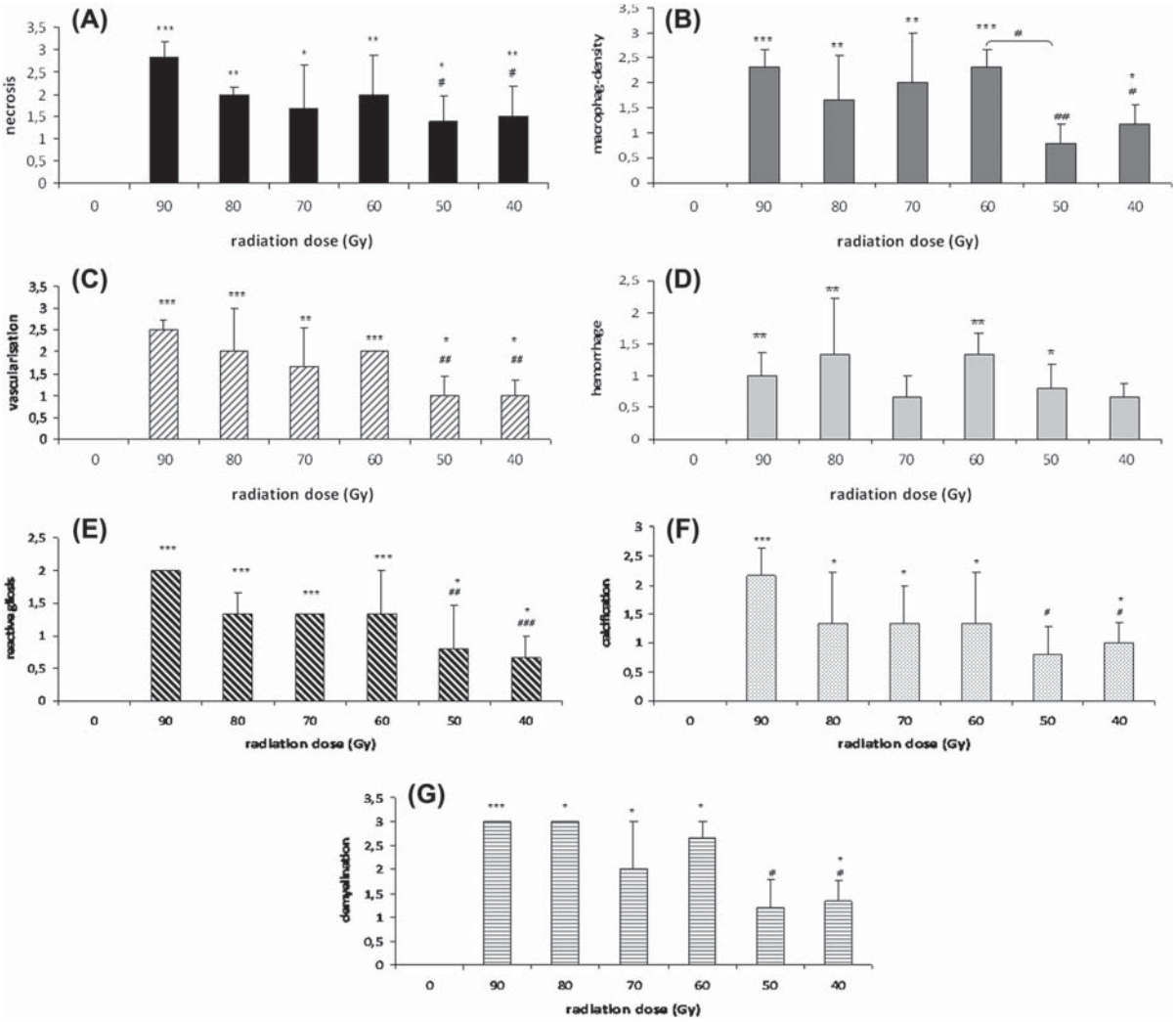

Figure 8 (A) In the irradiated region of the brain, the degree of necrosis correlated closely with the dose level (mean ± SEM, $n_{co} = 15$, $n_{40Gy} = 6$, $n_{50Gy} = 4$, $n_{60Gy} = 3$, $n_{70Gy} = 6$, $n_{80Gy} = 3$, $n_{90Gy} = 6$). n_{co} = number of conrol rats, n_{xGy} = number of rats irradiated at the x Gy dose level. Significance level between control and irradiated groups is indicated by *; and significance level between 90 Gy group and remain irradiated groups by #. (B) The numbers of foamy macrophages were significantly elevated relative to the control animals in all groups (mean ± SEM, $n_{co} = 15$, $n_{40Gy} = 6$, $n_{50Gy} = 4$, $n_{60Gy} = 3$, $n_{70Gy} = 6$, $n_{80Gy} = 3$, $n_{90Gy} = 6$). (C) A significant correlation was detected in the degree of vascularization in the irradiated volume between the control and the 90 Gy group (mean ± SEM, $n_{co} = 15$, $n_{40Gy} = 6$, $n_{50Gy} = 4$, $n_{60Gy} = 3$, $n_{70Gy} = 6$, $n_{80Gy} = 3$, $n_{90Gy} = 6$). (D) Relative to the control group, the level of hemorrhage was significantly increased in all groups except those that received 70 Gy or 40 Gy (mean ± SEM, $n_{co} = 15$, $n_{40Gy} = 6$, $n_{50Gy} = 4$, $n_{60Gy} = 3$, $n_{70Gy} = 6$, $n_{80Gy} = 3$, $n_{90Gy} = 6$). (E) The degree of reactive astrogliosis was significantly elevated in all the irradiated groups compared to the control animals (mean ± SEM, $n_{co} = 15$, $n_{40Gy} = 6$, $n_{50Gy} = 4$, $n_{60Gy} = 3$, $n_{70Gy} = 6$, $n_{80Gy} = 3$, $n_{90Gy} = 6$). (F) A significant correlation was detected in the degree of calcification in the irradiated volume between the control and the group irradiated at 90–120 Gy dose level, at 60–80 Gy dose level and at 40–50 Gy dose level (mean ± SEM, $n_{co} = 15$, $n_{40Gy} = 6$, $n_{50Gy} = 4$, $n_{60Gy} = 3$, $n_{70Gy} = 6$, $n_{80Gy} = 3$, $n_{90Gy} = 6$). (G) The higher doses caused severe demyelination, with destruction of the fibers, and the intermediate doses led to severe-to-moderate demyelination, while the lower doses resulted in only mild-to-moderate demyelination (mean ± SEM, $n_{co} = 15$, $n_{40Gy} = 6$, $n_{50Gy} = 4$, $n_{60Gy} = 3$, $n_{70Gy} = 6$, $n_{80Gy} = 3$, $n_{90Gy} = 6$).

We performed a dose-de-escalation from 120–40 Gy in 10-Gy steps. The morphological and functional changes detected were clearly related to the radiation dose. The two-weekly assessment of open-field tests did not reveal any behavioural alteration, apart from the rats irradiated at 120–110 Gy, which displayed an obvious deterioration. Only the changes in prancing activity indicated the effect of the focal brain injury; these were first observed 40–55 days post-irradiation at the 90 Gy dose level. In the course of its explorations, the rat gains information about its environment and it continues this activity until it can develop an integrated concept of the situation. One of the most important roles of the hippocampus is to achieve this integration, and in normal rats this goes well. Rats with an impaired dorsal hippocampus require more extensive exploration to attain the same result. The changes in spontaneous locomotor activity mostly depend on the nature and magnitude of the lesions (Leggio et al. 2006, Alstott et al. 2009). In our experiments, the slight changes in locomotor activity can be explained by the short time frame of the open-field tests. These revealed that the effects of relevant damage in the motor cortex start to become observable 8 weeks after irradiation, which corresponds well to the development of an irreversible human focal brain injury (Godsil et al. 2005, Huang et al. 2009, Caceres et al. 2010). Nevertheless, we do not consider the open-field activity to be a highly sensitive tool for the detection of changes due to radiation damage.

A subsequent detailed analysis of our data demonstrated that the locomotor deterioration could be measured at high dose levels and at later time points than 2 months after the

treatment. In planned studies, therefore, we intend to perform open-field tests at two-week intervals up to 6 months. The MWM test is widely used for the detection of neurofunctional impairments (Justino et al. 1997, Yoneoka et al. 1999, Akiyama et al. 2001, Liscák et al. 2002, Vorhees and Williams 2006, Jirák et al. 2007, Shi et al. 2011). In our model, the memory decline first appeared between 30 and 120 days after the irradiation, clearly depending on the dose delivered. The behavioural impairment correlated closely with the morphological changes detected by MRI and histology. Numerous publications have described different methods and reported on the value of MRI examinations for the detection of changes (even at a molecular level) due to ionizing radiation in a small-animal brain. Radiation-induced morphological changes demonstrated by repeated MRI scans correlated well with the dose, the duration and location of the lesion (Karger et al. 1997, Ishikawa et al. 1999, Brisman et al. 2003). Single doses of 150 Gy or 100 Gy produced necrosis in the hippocampus within 1–3 months (Liscák et al. 2002), and 75 Gy caused a focal brain lesion within 3–6 months (Liscák et al. 2002, Jirák et al. 2007). At doses higher than 60 Gy, necrotic changes started to appear within 6 months (Liscák et al. 2002, Brisman et al. 2003), and 20 months after lower doses, such as 25–50 Gy, delivered to the right frontal lobe of rats, MRI changes were demonstrated in relaxation times T1 and T2 (Karger et al. 1997, Ishikawa et al. 1999).

We set out to perform simultaneous MRI examinations on six rats with the available 1.5 T device and a human brain coil in order to detect and follow up the necrotic changes in vivo, and to optimize the time point of histopathologic examinations. Our method proved simple and effective, with a relatively high throughput, and the results exhibited a clear correspondence with the histopathological findings. The H&E slides showed that the irradiation was localized to a defined small brain volume and the effects in the animals were well-reproducible: The damage appeared only in the irradiated region. We did not observe histopathological aberrations in the contralateral hemisphere or in the control animals. This proves the efficacy of the irradiation method. The induced changes depended strongly on the radiation dose. Significant correlations were detected between the radiation dose and the degree of necrosis, the presence of foamy macrophages, the vascularization and the calcification.

Previous studies have indicated that histopathological structural changes, involving a decrease in the cell number and demyelination, can be expected in the dose range 50–100 Gy (Kamiryo et al. 2001, Liscák et al. 2002, Ernst-Stecken et al. 2007). With such doses, our histopathological analysis revealed measurable 6×8 mm necrotic lesions with cysta ex emollition, hemorrhage and a reactive cellular response. In confirmation of earlier data (Münter et al. 1999, Liscák et al. 2002, Jirák et al. 2007, Kumar et al. 2012), the severity of the radiation damage was strictly dose-dependent.

Conclusions

We have developed a well-reproducible small-animal radiation model that results in dose-dependent focal brain damage, as confirmed by behavioural tests, in vivo MRI examinations and histopathological evaluation. The effects were strongly dose-dependent and verifiable from both functional and morphological aspects. This model could be used to study the modifying effects of radiation on neurofunctioning.

Declaration of interest

The authors declare that the research was conducted in the absence of any commercial or financial relationships that could be construed as a potential conflict of interest. The authors alone are responsible for the content and writing of the paper.

This research project was supported by Országos Tudományos Kutatási Alapprogramok (OTKA) grant 75833, and "TÁMOP-4.2.1/B-09/1/KONV-2010-0005 – Creating the Centre of Excellence at the University of Szeged", supported by the European Union and co-financed by the European Regional Development Fund.

References

Akiyama K, Tanaka R, Sato M, Takeda N. 2001. Cognitive dysfunction and histological findings in adult rats one year after whole brain irradiation. Neurologia Medico-Chirurgica 41:590–598.

Alstott J, Breakspear M, Hagmann P, Cammoun L, Sporns O. 2009. Modeling the impact of lesions in the human brain. PLoS Computational Biology 5:e1000408.

Anschel DJ, Romanelli P, Benveniste H, Foerster B, Kalef-Ezra J, Zhong Z, Dilmanian FA. 2007. Evolution of a focal brain lesion produced by interlaced microplanar X-rays. Minimally Invasive Neurosurgery 50:43–46.

Belka C, Budach W, Kortmann RD, Bamberg M. 2001. Radiation induced CNS toxicity: Molecular and cellular mechanisms. British Journal of Cancer 85:1233–1239.

Blonigen BJ, Steinmetz RD, Levin L, Lamba MA, Warnick RE, Breneman JC. 2010. Irradiated volume as a predictor of brain radionecrosis after linear accelerator stereotactic radiosurgery. International Journal of Radiation Oncology Biology Physics 77:996–1001.

Brisman JL, Cole AJ, Cosgrove GR, Thornton AF, Rabinov J, Bussiere M, Bradley-Moore M, Hedley-Whyte T, Chapman PH. 2003. Radiosurgery of the rat hippocampus: Magnetic resonance imaging, neurophysiological, histological, and behavioral studies. Neurosurgery 53:951–961.

Caceres LG, Aon Bertolino L, Saraceno GE, Zorrilla Zubilete MA, Uran SL, Capani F, Guelman LR. 2010. Hippocampal-related memory deficits and histological damage induced by neonatal ionizing radiation exposure. Role of oxidative status. Brain Research 1312:67–78.

Charest G, Mathieu D, Lepage M, Fortin D, Paquette B, Sanche L. 2009. Polymer gel in rat skull to assess the accuracy of a new rat stereotactic device for use with the Gamma Knife. Acta Neurochirurgica (Wien) 151:677–683.

Chua DT, Wu SX, Lee V, Tsang J. 2009. Comparison of single versus fractionated dose of stereotactic radiotherapy for salvaging local failures of nasopharyngeal carcinoma: A matched-cohort analysis. Head and Neck Oncology 1:13.

Emami B, Lyman J, Brown A, Coia L, Goitein M, Munzenrider JE, Shank B, Solin LJ, Wesson M. 1991. Tolerance of normal tissue to therapeutic irradiation. International Journal of Radiation Oncology Biology Physics 21:109–122.

Ernst-Stecken A, Jeske I, Hess A, Rödel F, Ganslandt O, Grabenbauer G, Sauer R, Brune K, Blümcke I. 2007. Hypofractionated stereotactic radiotherapy to the rat hippocampus. Determination of dose response and tolerance. Strahlentherapie und Onkologie 183:440–446.

Farkas R, Kovács P, Aradi M, Bellyei SZ, Weiczner R, Kalincsák J, Sebestyén ZS, Hideghéty K. Single, high dose irradiation of defined region of rat brain with stereotactic BrainLab system (ahead of publication).

Fike JR, Rosi S, Limoli CL. 2009. Neural precursor cells and central nervous system radiation sensitivity. Seminars in Radiation Oncology 19:122–132.

Fike JR, Sheline GE, Cann CE, Davis RL. 1984. Radiation necrosis. Progress in Experimental Tumor Research 28:136–151.

Godsil BP, Stefanacci L, Fanselow MS. 2005. Bright light suppresses hyperactivity induced by excitotoxic dorsal hippocampus lesions in the rat. Behavioral Neuroscience 119:1339–1352.

Gutman G, Strumban E, Sozontov E, Jenrow K. 2007. X-ray scalpel – a new device for targeted x-ray brachytherapy and stereotactic radiosurgery. Physics in Medicine and Biology 52:1757–1770.

Hirano M, Shibato J, Rakwal R, Kouyama N, Katayama Y, Hayashi M, Masuo Y. 2009. Transcriptomic analysis of rat brain tissue following gamma knife surgery: Early and distinct bilateral effects in the unirradiated striatum. Molecules and Cells 27:263–268.

Huang Y, Brandon MP, Griffin AL, Hasselmo ME, Eden UT. 2009. Decoding movement trajectories through a T-maze using point process filters applied to place field data from rat hippocampal region CA1. Neural Computation 21:3305–3334.

Hwang SY, Jung JS, Kim TH, Lim SJ, Oh ES, Kim JY, Ji KA, Joe EH, Cho KH, Han IO. 2006. Ionizing radiation induces astrocyte gliosis through microglia activation. Neurobiology of Disease 21:457–467.

Ishikawa S, Otsuki T, Kaneki M, Jokura H, Yoshimoto T. 1999. Dose-related effects of single focal irradiation in the medial temporal lobe structures in rats – magnetic resonance imaging and histological study. Neurologia Medico-Chirurgica (Tokyo) 39:1–7.

Jenrow KA, Brown SL, Liu J, Kolozsvary A, Lapanowski K, Kim JH. 2010. Ramipril mitigates radiation-induced impairment of neurogenesis in the rat dentate gyrus. Radiation Oncology 5:6.

Jirák D, Náměstková K, Herynek V, Liscák R, Vymazal J, Mares V, Syková E, Hájek M. 2007. Lesion evolution after gamma knife irradiation observed by magnetic resonance imaging. International Journal of Radiation Biology 83:237–244.

Justino L, Welner SA, Tannenbaum GS, Schipper HM. 1997. Long-term effects of cysteamine on cognitive and locomotor behaviour in rats: Relationship to hippocampal glial pathology and somatostatin levels. Brain Research 761:127–134.

Kamiryo T, Han K, Golfinos J, Nelson PK. 2001. A stereotactic device for experimental rat and mouse irradiation using gamma knife model B – technical note. Acta Neurochirurgica (Wien) 143:83–87.

Karger CP, Hartmann GH, Peschke P, Debus J, Hoffmann U, Brix G, Hahn EW, Lorenz WJ. 1997. Dose-response relationship for late functional changes in the rat brain after radiosurgery evaluated by magnetic resonance imaging. International Journal of Radiation Oncology Biology Physics 39:1163–1172.

Kase Y, Himukai T, Nagano A, Tameshige Y, Minohara S, Matsufuji N, Mizoe J, Fossati P, Hasegawa A, Kanai T. 2011. Preliminary calculation of RBE-weighted dose distribution for cerebral radionecrosis in carbon-ion treatment planning. Journal of Radiation Research 52:789–796.

Kumar S, Arbab AS, Jain R, Kim J, deCarvalho AC, Shankar A, Mikkelsen T, Brown SL. 2012. Development of a novel animal model to differentiate radiation necrosis from tumor recurrence. Journal of Neuro-oncology 108:411–420.

Leggio MG, Federico F, Neri P, Graziano A, Mandolesi L, Petrosini L. 2006. NMDA receptor activity in learning spatial procedural strategies I. The influence of hippocampal lesions. Brain Research Bulletin 70:347–355.

Liang CD, Li WL, Liu N, Yin Y, Hao J, Zhao WQ. 2008. Effects of gamma knife irradiation on the expression of NMDA receptor subunits in rat forebrain. Neuroscience Letters 439:250–255.

Lin Y, Limoli C, Acharya M, Christie L, Bosch O, Kumar V, Hamamura M, Roa D. 2012. SU-E-T-271: Irradiating a single hippocampus in a small rodent using VMAT- RapidArc SRS: Preliminary data. Medical Physics 39:3765–3766.

Liscák R, Vladyka V, Novotný J Jr, Brozek G, Naměstkova K, Mares V, Herynek V, Jirák D, Hájek M, Syková E. 2002. Leksell gamma knife lesioning of the rat hippocampus: The relationship between radiation dose and functional and structural damage. Journal of Neurosurgery 97:666–673.

Lunsford LD, Altschuler EM, Flickinger JC, Wu A, Martinez AJ. 1990. In vivo biological effects of stereotactic radiosurgery: A primate model. Neurosurgery 27:373–382.

Marcelin B, Kjäll P, Johansson J, Lundin A, Nordström H, Eriksson M, Bernard C, Régis J. 2010. Using Monte-Carlo-simulated radiation transport to calculate dose distribution in rats before irradiation with Leksell Gamma Knife 4C: Technical note. Stereotactic and Functional Neurosurgery 88:208–215.

Marks LB, Yorke ED, Jackson A, Ten Haken RK, Constine LS, Eisbruch A, Bentzen SM, Nam J, Deasy JO. 2010. Use of normal tissue complication probability models in the clinic. International Journal of Radiation Oncology Biology Physics 76:S10–9.

Massager N, Maris C, Nissim O, Devriendt D, Salmon I, Levivier M. 2009a. Experimental analysis of radiation dose distribution in radiosurgery: I. Dose hot spot inside target volume. Stereotactic and Functional Neurosurgery 87:82–87.

Massager N, Maris C, Nissim O, Devriendt D, Salmon I, Levivier M. 2009b. Experimental analysis of radiation dose distribution in radiosurgery. II. Dose fall-off outside the target volume. Stereotactic and Functional Neurosurgery 87:137–142.

Minniti G, Clarke E, Lanzetta G, Osti MF, Trasimeni G, Bozzao A, Romano A, Enrici RM. 2011. Stereotactic radiosurgery for brain metastases: Analysis of outcome and risk of brain radionecrosis. Radiation Oncology 6:48.

Mizumoto M, Tsuboi K, Igaki H, Yamamoto T, Takano S, Oshiro Y, Hayashi Y, Hashii H, Kanemoto A, Nakayama H, Sugahara S, Sakurai H, Matsumura A, Tokuuye K. 2010. Phase I/II trial of hyperfractionated concomitant boost proton radiotherapy for supratentorial glioblastoma multiforme. International Journal of Radiation Oncology Biology Physics 77:98–105.

Monje ML, Palmer T. 2003. Radiation injury and neurogenesis. Current Opinion in Neurology 16:129–134.

Münter MW, Karger CP, Reith W, Schneider HM, Peschke P, Debus J. 1999. Delayed vascular injury after single high-dose irradiation in the rat brain: Histologic immunohistochemical, and angiographic studies. Radiology 212:475–482.

Münter MW, Karger CP, Schröck H, de Vries A, Schneider HM, Wannenmacher M, Debus J. 2001. Late radiation changes after small volume radiosurgery of the rat brain. Measuring local cerebral blood flow and histopathological studies. Strahlentherapie und Onkologie 177:354–361.

Namba H, Irie T, Fukushi K, Iyo M, Hashimoto T, Ando K. 1996. Time courses of changes in cerebral blood flow and blood-brain barrier integrity by focal proton radiation in the rat. Neurological Research 18:83–86.

Panagiotakos G, Alshamy G, Chan B, Abrams R, Greenberg E, Saxena A, Bradbury M, Edgar M, Gutin P, Tabar V. 2007. Long-term impact of radiation on the stem cell and oligodendrocyte precursors in the brain. PLoS One 2:e588.

Rabinov JD, Cheng LL, Lee PL, Brisman JL, Loeffler JS, Cole AJ, Cosgrove GR, Bussiere MR, Chaves T, Gonzalez RG. 2006. MR spectroscopic changes in the rat hippocampus following proton radiosurgery. Stereotactic and Functional Neurosurgery 84:147–154.

Reinacher PC, Blum C, Gass P, Karger CP, Debus J. 1999. Quantification of microglial late reaction to stereotactic irradiation of the rat brain using computer-aided image analysis. Experimental Neurology 160:117–123.

Robbins ME, Zhao W, Garcia-Espinosa MA, Diz DI. 2010. Renin-angiotensin system blockers and modulation of radiation-induced brain injury. Current Drug Targets 11:1413–1422.

Ruben JD, Dally M, Bailey M, Smith R, McLean CA, Fedele P. 2006. Cerebral radiation necrosis: Incidence, outcomes, and risk factors with emphasis on radiation parameters and chemotherapy. International Journal of Radiation Oncology Biology Physics 65:499–508.

Shi L, Olson J, D'Agostino R Jr, Linville C, Nicolle MM, Robbins ME, Wheeler KT, Brunso-Bechtold JK. 2011. Aging masks detection of radiation-induced brain injury. Brain Research 1385:307–316.

Spiegelmann R, Friedman WA, Bova FJ, Theele DP, Mickle JP. 1993. LINAC radiosurgery: An animal model. Journal of Neurosurgery 78:638–644.

Tan YF, Rosenzweig S, Jaffray D, Wojtowicz JM. 2011. Depletion of new neurons by image guided irradiation. Frontiers in Neuroscience 5:59.

Tiller-Borcich JK, Fike JR, Phillips TL, Davis RL. 1987. Pathology of delayed radiation brain damage: An experimental canine model. Radiation Research 110:161–172.

Tofilon PJ, Fike JR. 2000. The radioresponse of the central nervous system: A dynamic process. Radiation Research 153:357–370.

Vinchon-Petit S, Jarnet D, Jadaud E, Feuvret L, Garcion E, Menei P. 2010. External irradiation models for intracranial 9L glioma studies. Journal of Experimental & Clinical Cancer Research 29:142.

Vorhees CV, Williams MT. 2006. Morris water maze: Procedures for assessing spatial and related forms of learning and memory. Nature Protocols 1:848–858.

Williams BJ, Suki D, Fox BD, Pelloski CE, Maldaun MV, Sawaya RE, Lang FF, Rao G. 2009. Stereotactic radiosurgery for metastatic brain tumors: A comprehensive review of complications. Journal of Neurosurgery 111:439–448.

Wong CS, Van der Kogel AJ. 2004. Mechanisms of radiation injury to the central nervous system: Implications for neuroprotection. Molecular Interventions 4:273–284.

Xin N, Li YJ, Li X, Wang X, Li Y, Zhang X, Dai RJ, Meng WW, Wang HL, Ma H, Schläppi M, Deng YL. 2012. Dragon's blood may have radioprotective effects in radiation-induced rat brain injury. Radiation Research 178:75–85.

Yamaguchi N, Yamashima T, Yamashita J. 1991. A histological and flow cytometric study of dog brain endothelial cell injuries in delayed radiation necrosis. Journal of Neurosurgery 74:625–632.

Yang T, Wu SL, Liang JC, Rao ZR, Ju G. 2000. Time-dependent astroglial changes after gamma knife radiosurgery in the rat forebrain. Neurosurgery 47:407–415.

Yoneoka Y, Satoh M, Akiyama K, Sano K, Fujii Y, Tanaka R. 1999. An experimental study of radiation-induced cognitive dysfunction in an adult rat model. British Journal of Radiology 72:1196–1201.